# JAAS

Accepted Manuscript


This is an *Accepted Manuscript*, which has been through the Royal Society of Chemistry peer review process and has been accepted for publication.

*Accepted Manuscripts* are published online shortly after acceptance, before technical editing, formatting and proof reading. Using this free service, authors can make their results available to the community, in citable form, before we publish the edited article. We will replace this *Accepted Manuscript* with the edited and formatted *Advance Article* as soon as it is available.

You can find more information about *Accepted Manuscripts* in the Information for Authors.

Please note that technical editing may introduce minor changes to the text and/or graphics, which may alter content. The journal's standard Terms & Conditions and the Ethical guidelines still apply. In no event shall the Royal Society of Chemistry be held responsible for any errors or omissions in this *Accepted Manuscript* or any consequences arising from the use of any information it contains.

ROYAL SOCIETY OF CHEMISTRY

www.rsc.org/jaas

# Considerations of Inductively Coupled Plasma Mass Spectrometry Techniques for Characterizing the Dissolution of Metal-Based Nanomaterials in Biological Tissues

Cheng-Kuan Su and Yuh-Chang Sun*

Department of Biomedical Engineering and Environmental Sciences, National Tsing-Hua University, Hsinchu, 30013, Taiwan.

## Abstract

Dissolution of metal-based nanomaterials (MNMs) leads to the release of metal ion species; this phenomenon is a major concern affecting the widespread application of MNMs because it can affect their subsequent biodistribution patterns and toxic responses toward living biological systems. It is crucial that we thoroughly understand the dissolution behavior and chemical fate—and associated health effects—of MNMs when assessing their safety considerations. To date, however, quantitative characterization of the transformations of MNMs within living animal bodies has remained a methodological challenge. In this Review, we address the technical issues, the state of the art, and the limitations of currently available sample preparation procedures, as well as the various differentiation schemes coupled with inductively coupled plasma mass spectrometry (ICP-MS) techniques for analysis, that have been employed to reveal MNM dissolution in complicated biological tissue samples. In addition, we highlight the importance of developing new analytical strategies for ICP-MS to facilitate unbiased investigations into the dissolution behavior of MNMs with respect to their long-term biological effects and nanotoxicological properties.

* To whom correspondence should be addressed.

Fax: +886-3-5723883, Tel.: +886-3-5727309

e-mail: ycsun@mx.nthu.edu.tw

## 1. Introduction

As metal-, metal oxide-, and metalloid-containing materials having at least one dimension between 1 and 100 nm,[1, 2] metal-based nanomaterials (MNMs) exhibit unique physicochemical properties because of their small sizes, large surface areas, and distinct chemical reactivity.[3–5] During the last decade, interest in engineered MNMs—including gold nanoparticles (AuNPs), silver nanoparticles (AgNPs), zinc oxide nanoparticles (ZnO NPs), titanium dioxide NPs, iron oxide NPs, and quantum dots (QDs)—has increased; this advancement has led to many innovative consumer products appearing in our daily lives[6, 7] as well as advancing nano-biomedicine as a rapidly growing research field.[8–10] Accompanied by their rapid commercialization and production, human exposure to MNMs is growing—through inhalation, dermal contact, oral ingestion, and medical administration.[11, 12] To date, however, there is a shortage of available data and a lack of appropriate analytical techniques to examine the risks caused by exposure to xenobiotic nanomaterials (NMs); we will require a better understanding of their biodistribution behavior and dose–response properties if we are to characterize their toxic effects. To investigate the adsorption, distribution, metabolism, and excretion (ADME) of these MNMs and their associated metal ion species, we must identify the toxic potential and health effects of MNMs and balance them with respect to their favorable novel properties.[13–15]

The toxic effects of MNMs are related their size, shape, surface properties, and chemical compositions.[16–19] Nevertheless, the interrelations between these physicochemical properties and the resulting toxicity of MNMs in living animals remain unresolved, because it is difficult to predict the toxic effects and damage caused by

MNMs through recapitulation of known toxic mechanisms at cellular levels.[17] The transformations and fates of MNMs are very complex, but can be classified broadly into two states: residual nanostructures and released metal ion species.[19, 20]

When they remain in the form of intact nanoparticulate matter, MNMs in biological systems can adhere to organ cells to influence membrane properties or penetrate into intracellular space to interrupt normal cell functions; alternatively, after they have dissolved, their ionic species can inactivate or compromise the functionality of vital enzymes.[15] Therefore, if exposed MNMs persist or do not meet the criteria for being excreted via renal and hepatic clearance,[21–23] it is believed that the physiological responses to MNMs finally should be similar to the species associated to their chemical compositions.[24] For QDs, for example, concerns about their toxicity are attributed mainly to their degradation and release of notorious heavy metals (e.g., Cd ions), despite several QD toxicity studies having demonstrated minimized adverse effects in living rats and primates.[25–27] Accordingly, the dissolution of MNMs is dependent on the metal ions' solubility and association with available ligands in a given aqueous medium (possessing various ionic strengths, pH, and existing biological molecules), the concentration gradient between the particle's surfaces and the phase of the bulk solution, and the aggregation states of the MNMs. MNMs of smaller sizes and higher surface-to-volume ratios can also display peculiar physicochemical properties that are responsible for their reactivity, dissolution, and interactions with biological components.[24, 28] In addition, reactive oxygen species generated during their metabolic processes can also accelerate the dissolution effects of MNMs in living biological systems.[28] Evaluating the intrinsic stabilities of the chemical compositions of MNMs and examining whether metal ion species are released

are both important processes when determining their nanotoxicological properties and biomedical applications. For the reasons described above, without clear knowledge of the chemical fate of MNMs after their exposure, the prediction of the potential toxicity of MNMs toward biological system cannot be concluded.

Prior to studying the site-specific toxic effects of MNMs and their released ion species in living animals, it would be indispensable to comprehensively understand the biodistribution of these MNMs. Because studying the biodistribution of a certain kind of MNMs usually requires collecting a large amount of quantification data from many administered individuals, there is great need for the development of more efficient and sensitive analytical strategies for the high-throughput and accurate analyses of MNMs in a large number of animal samples. Current approaches to evaluate the time-dependent accumulation of these exposed MNMs in animal tissues involve (i) measuring photon emissions from the MNMs themselves (e.g., QDs), or that indirectly from the additionally labeled fluorescent dyes or radioactive tracers on/in MNMs (e.g., using whole-body fluorescence imaging, single-photon emission computed tomography, positron emission tomography, or *ex vivo* gamma counting) or (ii) analyzing MNMs in digested animal tissues using conventional elemental analysis equipment [e.g., flame atomic absorption spectrometry, graphite furnace atomic absorption spectrometry, inductively coupled plasma optical emission spectrometry, inductively coupled plasma mass spectrometry (ICP-MS)].[29-33] Although imaging techniques are conveniently available to provide the spatial information, major concerns for labeling methods are the unanticipated or altered biodistribution resulted from the changes of MNM's physicochemical properties,[34-36] the occurrence of doubtful tracking and quantification of MNMs if the labeled photon-

emitting species detached in biological systems,[36, 37] and most importantly, limited information about the MNM's integrity which can be further revealed from their emitted photons.[38-40]

Compared with that, direct determination of the elements from MNMs based on elemental analysis techniques should be relatively less controversial for quantification of MNMs. After completely decomposing organ and tissue samples collected from animals exposed to MNMs, the biodistributions of the MNMs can be elucidated through determining the specific elements found within these MNMs. Moreover, combining suitable sample pretreatment procedures with adequate separation methods will further enable the evaluation of the full chemical fate of administered MNMs in complicated biological environments. Based on the comparisons among these elemental analysis instruments (Fig. 1), methods based on ICP-MS techniques have the great attractions of high sensitivity (detection limit of approximately ng $kg^{-1}$ for most elements), high selectivity, fewer interferences, wide linear dynamic range, multi-element/isotope analysis capability, fast data acquisition, high sample throughput, micro sample needed, and robustness, therefore placing them among the most powerful techniques to be popularly hyphenated with online/offline sample pretreatment procedures for routinely quantifying MNMs in biological tissues.[29-33, 41, 42]

Nanometallomics has been initiated as a new branch of metallomics; it is devoted to the identification, quantification, and chemical speciation of MNMs and their released metal ion species, as well as their health effects in biological systems.[28, 43] The demand for more sensitive, selective, and diverse analytical techniques to acquire the size and chemical information of these MNMs has recently been highlighted.[28, 29, 43, 44] As

summarized in Fig. 2, analyses of the fractions of released metal ions and residual MNMs within animal tissues, as well as studies of the long-term chemical fate of these MNMs, will play an essential role in assessing their consequent health effects and nanosafety, thereby facilitating the future development of MNM-related products. In this Review, we provide a brief summary of the recent reports focusing on the use of ICP-MS determination methods to address the chemical identification and dissolution behavior of MNMs in animal bodies. We also note the limitations in the current development of ICP-MS-based methods incorporated with diverse sample pretreatment procedures for studying the chemical fate of MNMs in living animals.

## 2. Use of ICP-MS techniques to study the biodistribution and chemical fate of MNMs

### 2.1 Capability of ICP-MS methods

For elements that are found in trace quantities or are not found natively in animal bodies (e.g., Ag, Au, Cd, Te) are exogenous substances, the accumulation sites and resulting biological effects of these exposed MNMs can be examined through their determination using an ICP mass spectrometer.[30–33, 44] Moreover, when the MNMs are composed of more than one metal or metalloid (e.g., CdSe, CdTe, CdHgTe, or InAs QDs), the intrinsic molar ratio of their chemical components is the best indicator to determine the integrity of their nanostructures.

For example, Lin *et al.* evaluated the chemical fate of QD705, a formulation of CdSeTe/ZnS QDs, by analyzing the molar ratios of Cd and Te in mouse liver, kidney, and spleen, and used the inducted metallothionein (MT) as a biomarker for the elevated level of Cd ions in mouse bodies.[45] Once the administered QD705 had dissolved, the released Cd ions were retained in tissues for a much longer period of time than were the Te ions, because Cd has a biological half-life that is approximately 10–12 times longer than that of Te in animal bodies. They observed (Fig. 3) increased Cd/Te ratios and MT-1 expression in mouse kidney from 2 to 16 weeks post-administration, evidently indicating the occurrence of QD705 dissolution and the redistribution of released Cd ions to the mouse kidney.

Han *et al.* also compared the biodistribution patterns of Cd and Te, from water-soluble CdTe QDs, in mice.[46] They observed differences between Cd and Te in terms of plasma

kinetics and tissue biodistribution, implying that CdTe QDs degraded or aggregated *in vivo* and concluding that the Cd content determined from plasma or tissue samples may not actually represent the biodistribution pattern of administered QDs.

For MNMs containing elements that are essential or relatively abundant in animal bodies (e.g., ZnO or iron oxide NPs), the applicability of ICP-MS to access their biodistribution data is limited because an ICP mass spectrometer is incapable of distinguishing exogenously administered elements from endogenous ones. Doping these MNMs with unusual metal tracers (e.g. lanthanide metals[47] or enriched stable isotopes[48-50]) or administering relatively higher dosages into living animals are alternatives that can be used to evaluate their biodistribution.[51, 52] Nevertheless, the leakage of dopant elements, or the abnormal accumulation of these MNMs in target and non-target tissues as a result of the higher administration dose, may be pharmaceutically irrelevant for their biomedical applications.

As mentioned above, conventional MNM biodistribution studies are performed by determining specific metal ions that are distinguishable from those found naturally in animal organ and tissues. The total concentration of one element found within a MNM may not exactly represent the time-dependent accumulation of this MNM in a biological tissue because their released metal ions and residual nanostructures may coexist. To date, toxicological studies of these MNMs toward living animals have connected their physicochemical properties and exposure routes to their biodistributions in living animals.[16] Little research has been undertaken to enable the chemical identification of these MNMs in living subjects,[45, 46] especially for examinations of their chemical fates and transformation species from initial exposure to final excretion.[53] In addition, at

present the toxic effects of MNMs, as attributed to their chemical compositions, are often evaluated by comparing the toxic responses of the simple ionic species from the tested MNMs and the intact nanostructures themselves.[45, 54–57] It is likely that the toxicity of the tested ion species may not actually reflect the effects of the MNMs, due to unidentified species formed during the transformation of the MNMs.

When using conventional sample introduction systems for ICP mass spectrometers, the harvested biological tissues for MNM biodistribution studies must usually be decomposed beforehand; nothing would be left regarding the integrity of any residual nanostructures. An unanswered issue is whether the toxicity of MNMs in living animals arises solely from their nanoparticulate form or from their released metal ions, or whether both are required.[58] We lack suitable sample pretreatment procedures that can mildly homogenize tissue samples while maintaining the physical and chemical properties of MNMs of interest and effectively differentiate dissolved metal ion species (from residual MNMs) from complicated biological matrices. For quantitative profiling of either released metal ions or residual MNMs in intact animal tissues and for evaluations of the species-dependent toxic effects associated with the chemical fate of MNMs, we must extend the capabilities of ICP-MS techniques by introducing appropriate sample pretreatment procedures combined with advanced differentiation schemes.[28, 43, 44]

### 2.2 Analytical considerations of current sample pretreatment schemes and coupled separation methods

When employing an ICP mass spectrometer to investigate MNMs, the collected biological tissues are often treated with strong acids or oxidants, such that any residual

nanostructures, if they existed, would also decompose. It should, therefore, be compulsory that, when studying the dissolution behaviors and chemical fates of MNMs in animal tissues, it be possible to liberate or extract the MNMs and their released species from the deposited tissues while maintaining their equilibrium status. Developing sample pretreatment procedures for studying MNM dissolution is a seriously challenging task because changes to the MNMs, due to a dilution process during sample pretreatment, or the existing biological ligands, potentially accelerating the dissolution of MNMs, may bias their resulting dissolution behavior.[59] Table 1 lists the methods available to homogenize, solubilize, or digest biological tissues to enable further characterization of tested MNMs and their released ion species. These techniques can be divided into three main groups: sonication-assisted homogenization, alkaline treatment, and enzyme digestion.

The sonication process can enhance the efficacy of traditional mechanical homogenization of biological tissue samples.[74, 75] By placing a specially designed acoustical tool or probe directly into an extraction buffer, which had been mixed with fine tissue powders of the collected tissues ground in a liquid $N_2$ bath, this convenient sample preparation method can be applied to liberate MNMs and their released metal ions from biological tissues.[60–63] The concern when using this sample pretreatment procedure is that the stability and integrity of the MNMs may be altered during sonication and the following extraction step.[62, 76, 77] In addition, the incomplete homogenization of biological tissues, partial extraction of analytes, and the removal of analyte species attached to biological debris during the centrifugation process would make doubtful the accurate quantitative profiling of MNM dissolution in tissue samples.[60]

Alternatively, alkaline treatment with a tetramethylammonium hydroxide (TMAH) solution has been used to completely or partially liberate AgNPs, AuNPs, QDs, carbon nanotubes (CNTs), and their dissolved metal ions from animal tissues.[63–71, 78] As a water-soluble strong base, TMAH enables the hydrolytic cleavage and methylation of ester, amide, and some ether bonds, as well as the breaking of disulfide chemical bonds, in biomolecules; therefore, it has been employed for the speciation of trace elements through atomic spectrometric techniques.[79–82] This treatment method has proven to yield high recoveries in terms of both particle number and total mass, relative to sonication-assisted tissue homogenization, and is promising for analyzing MNMs in biological tissue samples.[65] Rather than the undesired dissolution of MNMs that can occur under acidic treatment conditions, the methodological consideration of alkaline treatment is that the basic aqueous conditions would induce precipitation of released metal ions and aggregation of residual MNMs. Thus, the stability of residual MNMs and released metal ion should be estimated cautiously when applying alkaline sample preparation.

Proteinase K, which can degrade proteins into amino acids, is proteolytically active in a broad pH range from 7.5 to 12; the enzymatic digestion of biological tissues with proteinase K has also been applied to digest animal tissues for the liberation of MNMs of interest.[66, 72, 73] Loeschner *et al*. applied both alkaline and enzyme treatment to extract intravenously administered 60-nm AuNPs from rat spleens for subsequent identification through single-particle ICP-MS (spICP-MS) analysis.[66] Their observed similar particle size distributions (PSDs) of AuNPs before and after performing the applied sample preparation procedures, suggesting that the size information of the administered AuNPs was maintained after both alkaline and enzyme treatment. The spike recovery of AuNPs

for the enzymatically digested spleen was, however, approximately four times lower than that of TMAH-treated samples; the quantification data for AuNPs from the alkaline-treated tissues were availably comparable with those determined from the samples after microwave-assisted digestion using aqua regia.

Handling animal tissues with suitable pretreatment procedures is the most critical step for further evaluation of the chemical fate of MNMs. Recently, treatment of animal tissues with alkaline Solvable™ solution (a mixture of dodecyldimethylamine oxide, secondary alcohol ethoxylate, and sodium hydroxide in water;[83, 84] used as a commercial tissue solubilizer to facilitate sample measurements for liquid scintillation counting) has been applied successfully to the extraction of AgNPs, QDs, and their released ions from intact biological tissues.[68, 69, 71] Doudrick *et al.* compared eight chemical treatment methods used commonly to extract metal ions from complex matrices—Solvable™, ammonium hydroxide, nitric acid, sulfuric acid, hydrochloric acid (HCl), hydrofluoric acid, hydrogen peroxide, and proteinase K—for liberating the CNTs from rat lung tissues.[78] Solvable™ proved to have the highest efficiency for solubilizing lung tissues while providing a high quantitative recovery of CNTs, due to its mild nature and presence of surfactants. Based on characterization through programmed thermal analysis and Raman spectroscopy, the extraction of CNTs using a two-step digestion procedure, combining both Solvable™ and proteinase K, resulted in no apparent structural damage and a recovery of 98 ± 15% of CNTs spiked in whole rat lung tissues. Although most MNMs have chemical properties dissimilar to those of CNTs and are readily dissolved and chelated in the presence of biomolecules, sample pretreatment processes

incorporating multiple steps or digestive reagents should be useful for the future liberation of MNMs from complex biological tissues.[64, 78]

Despite progress in sample pretreatment methods for the liberation of MNMs and released metal ions from animal tissues, characterization of MNM dissolution remains difficult. There are many analytical strategies and separation methods available to differentiate the fractions of dissolved metal ions from their residual nanostructures in simple aqueous media. For example, the level of released $Ag^+$ ions or ions associated with low or macromolecular matter, the most likely species contributing to the toxicity of AgNPs, can be identified through spICP-MS analysis, $Ag^+$-specific indicators, or $Ag^+$-selective electrodes; these ions can be separated from residual AgNPs using such the methods as centrifugation, ultrafiltration, liquid chromatography, and cloud point extraction (CPE).[85–90] Nevertheless, when these MNMs enter biological environments were rich in thiol- and phosphate-containing biomolecules, their surfaces will be covered by a thick layer of protein corona, causing them to exhibit a totally distinct chemical identity,[91-94] and their released metal ion species will tend to form complexes with small ligands and biomolecules.[20, 95, 96] Accordingly, the analytical methods mentioned above might provide a distorted view when differentiating between the two distinct metal species[64, 65, 67, 85, 86] because the chemical identities of MNMs and their released metal ions in biological systems might be completely unlike those of the as-synthesized ones. Hence, we recommend addressing several aspects when using ICP-MS to investigate dissolution behavior, biotransformation, and chemical fate of MNMs in living animals: (i) the biological tissue samples must be treated appropriately without altering the equilibrium status between the MNMs and their released metal ions; (ii) the biomolecule-

coated MNMs and biomolecule-bound released metal ions in the biological matrix must be differentiated effectively; (iii) the applied differentiation schemes must be sufficiently robust to be applied to many tissue samples; (iv) the differentiated fractions of the MNMs and released metal ions must be determined with comparable instrumental sensitivities. In the following sections, we review the differentiation schemes, in terms of online/offline coupling with ICP mass spectrometers and their employed sample pretreatment procedures, for examinations of the dissolution behavior and chemical fate of MNMs in biological tissue samples.

## 3. Separation methods coupled with ICP-MS for studies of the chemical fate of MNMs

After MNMs and their released metal ions have been liberated from biological tissues, the differentiation schemes used at present to reveal the dissolution behavior of the MNMs are based on either direct identification of the released fraction of metal ion species or the relative changes in the PSDs of the MNMs before and after exposure. They can be categorized into three main groups: direct characterization through spICP-MS analysis; physical size discrimination strategies; and advanced differentiation schemes relying on the dissimilar properties of released metal ions and residual MNMs.

### 3.1 spICP-MS analysis

When a suspension containing MNMs is diluted appropriately and introduced into an ICP mass spectrometer using a conventional nebulizer, transient flashes of the metal ions comprising the MNM can be detected within a sufficiently short dwell time as a result of individual ionization of each MNM in the plasma.[97–101] The number of pulses is directly correlated to the number concentration of MNMs, with the signal intensity of the detected pulse related to the mass and size (assuming a spherical shape) of each MNM. Online spICP-MS analysis is a straightforward means of directly identifying the dissolution of MNMs in a complex aqueous suspension by revealing the differences in PSDs between the pristine and weathered MNMs.[66, 102] This technique, developed initially by Degueldre *et al*.,[97] has recently been highlighted for its applications in environmental[98, 103] and biological media.[65, 66, 73] The main consideration when using spICP-MS analysis to characterize MNMs is the need to finely adjust each experimental parameter, such as the

concentration of analyzed MNMs, the instrument dwell time, and, most critically, the threshold for discriminating NP events from background signals since partial measurement or double counting of particle events are the known shortcomings in using this technique.[99, 100, 104–108] Besides, the improper estimation of transport efficiency (for example, via collecting the waste stream existing the spray chamber) is a major source of error in the calculation of MNM sizes, and alternatively, some methods for accurately calibrating their particle sizes exist (e.g., using reference nanoparticles of known particle size or suspension of known particle number concentration).[99, 100, 104, 108]

Gray *et al*. used the alkaline tissue extraction procedure and spICP-MS analysis to quantitatively characterize AuNPs and AgNPs in environmentally relevant biological tissues.[65] To liberate the exposed MNMs, samples of ground beef, *Daphnia magna*, and *Lumbriculus variegatus* spiked with AuNPs or AgNPs were treated with a TMAH solution to allow determination of the size distributions and mass concentrations of these two MNMs. They validated the mass- and number-based recoveries of the spiked AuNPs and AgNPs (83–121%) in these biological tissues; notably, no significant dissolution (i.e., no change in PSDs) occurred for either the AuNPs or AgNPs in the samples of extracted *D. magna* tissues within 48 h post-administration. Loeschner *et al*. also applied spICP-MS analysis to evaluate the PSDs of intravenously administered AuNPs in rat spleen samples treated with the alkaline and enzyme digestion methods; they observed no apparent dissolution of the AuNPs deposited in the rat spleens one day post-administration.[66]

Because the signal intensities of pulses are proportional to the number of metal atoms in each MNM, whereas the dissolved ions are large enough in number to produce pulse

signals of averaged constant intensity,[103, 109] the ability of spICP-MS analysis to discriminate residual MNMs from released metal ions depends significantly on the relative signal intensities of the two species and whether the NP events are distinguished from background signals (released ions and polyatomic interferences). It has been demonstrated that frequency plots with respect to measured intensities were independent for dissolved $Ag^+$ ions and AgNPs, with different profiles of Poisson and lognormal distributions, respectively.[109] Thus far, no analytical studies have applied spICP-MS analysis to simultaneously characterize dissolved ionic species and residual MNMs in treated or non-treated tissue samples.

### 3.2 Size discrimination strategy

Although use of spICP-MS analysis to directly characterize MNMs requires relatively minimal optimization in advance, this technique is highly dependent on the signal-to-noise ratio of the used ICP mass spectrometer, possibly leading to impossible identification of the differences between smaller MNMs (ca. 20 nm)[59, 107, 108] and dissolved ion species. To employ a highly-sensitive high resolution multi-collector ICP-MS instrument or a high temporal resolution ICP time-of-flight mass spectrometer may eventually be useful to ameliorate this problem and to perform isotopic analysis of individual particles.[110–112] Coupling size discrimination strategies with plasma spectrometry methods for differentiating either the released metal ions or the changes in the PSDs of residual MNMs has become an alternative means of investigating the dissolution behavior of MNMs. In principle, size-based separation techniques [e.g., centrifugation, membrane-based ultrafiltration, liquid chromatography, field-flow fractionation (FFF)] are suitable for differentiation of dissolved metal ion species from

residual MNMs. In a complicated biological system, however, the chemical identities of the two distinct metal species would change unavoidably, hindering practical differentiation between biomolecule-coated MNMs and biomolecule-bound metal ions.

### 3.2.1 Centrifugation

Centrifugation is one of the most commonly used separation techniques in colloid science. In an aqueous suspension, gravitational energy is commensurable with thermal energy for most MNMs; therefore, they can settle and be fractionated by adjusting the applied centrifugal forces that cause the particles to move radially away from the rotation axis.[85, 113–118] To applicability of centrifugation methods in investigations of the dissolution of MNMs leans on the efficiency of removing the particulate species from the supernatant,[70, 119, 120] a process that may be facilitated through adjusting the sample acidity or adding destabilizing agents to induce precipitation of residual MNMs.[38, 121] There are, however, uncertainties when using centrifugation methods—the incomplete removal of smaller MNMs (e.g., in the sub-5 nm regime) from the supernatant or the additional dissolution of MNMs prompted by the chemicals used during this pretreatment stage—that can lead to overestimation of the ionic fractions in the supernatant.[64] By comparison, the metal–protein complexes that result from the interactions of released metal ion species with biomolecules might possibly be removed from the supernatant during the centrifugation process due mainly to significant increase of the mass of these metal ion species, potentially leading to underestimation of the ionic species released upon MNM dissolution.

Chen *et al*. utilized a method of differential centrifugation coupled with ICP-MS to investigate the integrity and aggregation of water-soluble silica coated CdSeS QDs in mice liver and kidney by analyzing Cd amounts in the supernatant and deposition.[119] They proposed the precipitation of intact QDs in a dissociative state by ultracentrifugation (400,000 *g* for 150 min) but not by mild centrifugation (1500 *g* for 10 min), the precipitation of the QDs binding to bio-macromolecule or adhering to tissue (bound state) under mild condition, and no precipitation of Cd ions by the two used centrifugation conditions. A notable increase (38 to 82%) of QDs in bound state from 6 to 120 h post-administration was found in the liver homogenate, but most QDs in the kidney remained dissociative (85%, 6 h post-administration). Also, their results of spike analysis indicated the analytical biases of QDs in supernatant under mild centrifugation and Cd ions in the deposition for the two centrifugation conditions.

Arslan *et al.* used a centrifugation method to selectively determine the concentrations of free Cd ions and total Cd in the TMAH-treated liver and kidney of rats exposed to thiol-capped CdSe QDs.[70] To separate ionic and nanoparticulate species, the TMAH-treated samples were diluted with deionized water and mildly centrifuged; the supernatant was then re-centrifuged to completely eliminate suspended tissue and intact QDs from the samples. Arslan *et al.* verified that the used QDs aggregated, but without releasing any significant amount of Cd ions into the TMAH-treated solution; they found that the thiol-capped QDs were not fully stable in animal bodies because the rat liver and kidney both contain significant levels of free Cd ions, with the accumulation of up to 6.6 and 26.8% in total Cd concentrations even when the QDs were not exposed to UV-light prior to injection (Fig. 4). These results also suggested that Cd-containing QDs would be

most detrimental to the kidneys, which appeared to be the major repositories of free Cd ions.

### 3.2.2 Ultrafiltration

With their ability to differentiate diffusible ionic species released from tested MNMs by using a membrane having a well-defined molecular weight cut-off (MWCO), ultrafiltration and centrifugal ultrafiltration methods are straightforward practical means of investigating the dissolution of MNMs, even though they are usually time-consuming and performed offline in a batch-wise determination strategy.[90] To date, no consensus has been reached regarding the MWCO that is most appropriate to explicitly discriminate released ionic species; the fractions of dissolved ion species in biologically relevant media have been tested frequently using membranes having MWCOs ranging from 3 to 10 kDa.[62, 90, 122–131] On the other hand, once these MNMs dissolve, the released metal ions (e.g., $Ag^{+}$, $Au^{3+}$, $Cd^{2+}$, $Zn^{2+}$, $Fe^{2+}$/$Fe^{3+}$, $Ti^{4+}$) may complex with high-affinity thiol- or phosphate-containing biomolecules[43] to form high-molecular-weight $M^{n+}$-bound biomolecules; for example, the $Ag^{+}$-BSA complex having a molecular weight of approximately 67 kDa. As a result, any released metal ions strongly attached to or complexed with large biomolecules might be excluded by the membrane used, potentially resulting in underestimation of the level of released ion species in the filtrate.[68, 71, 132, 133]

In a couple of studies,[68, 71] we applied commercial centrifugal filters (MWCO: 3 kDa) as a common separation strategy to evaluate the fractions of candidate ion species ($Ag^{+}$, $Cd^{2+}$, dissolved Te species) released from AgNPs and CdSeTe/ZnS QDs in fetal bovine serum (FBS)-containing media. After differentiating the diffusible ion species in samples

prepared at various concentration ratios of $Ag^+/Ag_{total}$, $Cd^{2+}/Cd_{total}$, and $TeO_3^{2-}/Te_{total}$ (the total concentration for each element, including both the spiked metal ions and the intact MNMs), the slopes between the expected and practically measured ratios (ideally the value should be 1) for $Ag^+/Ag_{total}$, $Cd^{2+}/Cd_{total}$, and $TeO_3^{2-}/Te_{total}$ were 0.0008, 0.5726, and 0.8789, respectively. These values revealed that, due to interactions between the cationic metal species and sulfur- or phosphorus-containing compounds that were excluded by the 3-kDa membranes,[20, 134–138] the ability to use a physical size-discrimination strategy to separate diffusible metal ion species in the presence of an abundance of biomolecules was suppressed significantly, especially for cationic $Ag^+$ and $Cd^{2+}$ species. Even though $TeO_3^{2-}$, a candidate species evaluated for QD dissolution, is anionic, and its binding to biomolecules should be relatively weak,[136] there was still an error of 12% between the expected and measured ratios when using the ultrafiltration method. Accordingly, when evaluating with conventional ultrafiltration methods, the toxic effects of MNMs contributed from the released metal ion species might be overestimated to a dramatic degree because the interactions between freely dissolved metal ion species and complicated biological matrices might be ignored when interpreting the experimental data.[24, 119, 139]

### 3.2.3 Liquid chromatography

In liquid chromatography, analytes in a mobile phase are separated while passing over the stationary phase of a column, with separation based on differences in the partitions between the mobile and stationary phases. In contrast, separations through size exclusion chromatography (SEC) are based on differences in the particles' hydrodynamic volumes, such that small particles meander freely through the pores around the stationary phase

and, thereby, travel through the column slowly. Coupling liquid chromatography methods—namely SEC,[63, 113] hydrodynamic chromatography,[140–142] ion exchange chromatography,[143, 144] reverse-phase liquid chromatography,[145, 146] and capillary electrophoresis[147, 148]—with an ICP mass spectrometer makes it possible to directly size MNMs and their released metal ions species from various aqueous samples. Although this unsophisticated technique has been employed to study the transformation and chemical fates of MNMs in consumer products and environmental media,[141, 142, 144] it has rarely been exploited properly for analyses of biological systems.[63]

Loeschner *et al*. used an affinity HPLC- and an anion exchange HPLC-ICP-MS systems, and an *in situ* sulfite derivatization method for elemental Se followed by spectrophotometric measurements to evaluate the chemical fate and metabolites of BSA-stabilized amorphous $Se^0$ nanoparticles ($Se^0$NPs) in rat bodies.[53] The plasma and urine samples (diluted by mobile phase) prior to HPLC analysis were simply filtered; the liver, kidney, and feces for sulfite derivaization were treated by a homogenizer in the excess of ultra-pure water. Their results clearly showed that for $Se^0$NP exposure, selenosugar (Se-methylseleno-N-acetyl-galactosamine) and trimethylselenonium ion were the major species for urinary excretion, plasma selenoprotein P level was as important biomarker for its bioavailability, and elemental Se was detected in rat liver, kidney, and feces 28 days post-administration. Such pathways may include that $Se^0$NPs became dissolved and oxidized to inorganic oxoanions of Se.

Jiménez-Lamana *et al*. developed a hyphenated SEC-ICP-MS system for analyzing the silver species released from orally administered AgNPs in rat liver and kidney cytosols.[63] The harvested tissue samples were ground, sonicated, and extracted with an ammonium

acetate buffer, and then the supernatants, collected through a centrifugation process, were injected. They demonstrated (Fig. 5) that, in rat liver, the morphology of the silver chromatogram was independent of the exposure time (30–81 days post-administration), and that $Ag^+$ ions were bound predominantly to high-molecular-weight (70–25 kDa) proteins; in contrast, the ratios of the complexes with high-molecular-weight ligands to those with low-molecular-weight ligands increased in rat kidneys upon increasing the exposure time. This low-molecular-weight fraction was identified, through comparison with relevant standards, as the complex of $Ag^+$ ions with cysteine-rich MT; therefore, these results confirmed the presence of a $Ag^+$–biomolecule complex, as well as the oxidation and dissolution of AgNPs within living animal bodies.

### 3.2.4 Field-flow fractionation

Designed to separate complex macromolecular, colloidal, and particulate materials, FFF operates through differential displacement in a flowing stream of liquid that carries the separated components within a well-defined interaction field.[149, 150] The most used system, asymmetric flow FFF ($AF^4$), is a chromatography-like separation technique that is achieved through application of a perpendicular liquid flow applied to push NMs against the accumulation wall (a semi-permeable membrane on a ceramic frit). The fractionation of NMs occurs through the interplay between the forces of particle diffusion and of pushing the NMs against the membrane, leading to size-dependent elution behavior.[151–153] The advantages of the FFF technique are the ready collection and elution of highly uniform components or dissimilar components with the same diffusion coefficients from the channel outlet, allowing each collected fraction to be analyzed offline or online to obtain simultaneously both physical and chemical information for

each of the tested MNMs. According to this characteristic of the instrumental configuration, FFF can be used to reveal MNM dissolution by comparing the PSDs of the residual fraction[64, 69, 72, 151, 154-156] but not of the released metal ions.[122, 147, 150]

Schmidt *et al.* established an analytical platform by coupling an $AF^4$ system with multiangle light scattering (MALS), dynamic light scattering (DLS), and ICP-MS to quantitatively characterize the size and mass information for intravenously administered AuNPs (10 and 60 nm) in rat liver samples that were stabilized with BSA prior to TMAH treatment.[64] They found that the administered AuNPs could be liberated efficiently from the rat liver tissues, with extraction recoveries ranging from 86 to 123% of the total Au content when using the alkaline treatment method. Unfortunately, the liberated 10- and 60-nm AuNPs from the TMAH-treated liver tissue could not be fractionated through their constructed $AF^4$ system because of strong association between the AuNPs and undissolved tissue debris, leading to non-Brownian elution during the fractionation process. Therefore, the development of more suitable sample pretreatment schemes for liberating deposited AuNPs from biological tissues will be necessary to satisfy the current FFF methodology.

Loeschner *et al.* also evaluated the analytical performance of the $AF^4$ system coupled with ICP-MS for AgNP fractionation from the remaining matrix of chicken meat.[72] The AgNP-spiked meat samples that had been subjected to enzymolysis with proteinase K were injected into the established hyphenated $AF^4$-ICP-MS system. Using both spICP-MS analysis and TEM observation, they confirmed that there was no difference in the PSDs between the pristine AgNPs and those treated through proteinase K digestion, suggesting that enzymatic digestion can be a promising sample preparation method for

the liberation of MNMs from biological tissues. Even though the spike recoveries of the AgNPs reached up to 80%, the acquired fractogram described the non-ideal (i.e. early) elution behavior of the spiked AgNPs.

Coleman *et al*. combined a symmetrical flow FFF system with spICP-MS analysis to characterize AgNPs in sediment-exposed *L. variegatus*.[61] The sample of the filtrate acquired from the homogenate of *L. variegatus* [it had been diluted with deionized water, sonicated, centrifuged, and filtered (0.45 μm)] was fractionated through the FFF system and detected using online ICP-MS. The subsamples characterized by the FFF-ICP-MS system were subjected to spICP-MS analysis to obtain further size information for the residual particles. Coleman *et al*. observed mean particle diameters between 55 and 60 nm for the residual AgNPs in the tissues of *L. variegatus*. Although this size range was different from the sizes of the primary AgNPs (80 nm) as determined through FFF characterization, it was virtually identical to that of weathered AgNPs (60 nm) in a simple exposure condition of deionized water. These results suggested that some of the initial AgNPs remained intact in the tested organisms, with no apparent tendency for dissolution in animal exposure studies.

The limiting factors when assessing the PSDs of tested MNMs when using an FFF system are (i) the unavailability of suitable reference nanoparticles for accurate size calibration of target MNMs, (ii) the undesirable sample dilution within fractionation channels when applying to tiny amount of samples with low concentration of MNMs, and (iii) the paucity of appropriate sample pretreatment procedures that allow the practical introduction of treated biological samples into the FFF device without altering the elution behavior of the MNMs during the fractionation process. In addition, unpredictable

particle–membrane interactions, resulting from electrostatic interactions between the surface of the flow channel membrane and the charged MNMs, often lead to unacceptable analyte recoveries and non-ideal elution behavior in most of the assessed $AF^4$ systems.[64, 72] The development of appropriate sample pretreatment methods, the use of a stepwise pre-fractionation step, and optimization of the elution process to minimize unwanted adhesion of MNMs onto the separation membrane are three potential approaches for improving the coupling of ICP-MS with FFF techniques for studies of the dissolution behavior and chemical fate of MNMs, thereby allowing such methods to be used to quantitatively characterize these administered MNMs in complicated biological tissue samples.

### 3.3 Advanced differentiation methods

In biological environments, the physicochemical properties of MNMs and the metal ions released from their dissolution are completely different. The use of size discrimination methods would be intrinsically obstructed because of the interplay among the coexisting biological matrix, the residual MNMs, and the released metal ions species. Advancements in separation techniques, with the aim of differentiating biomolecule-coated MNMs from biomolecule-bound metal ions in treated tissue samples, will be crucial for extending ICP-MS techniques to the identification of the chemical fate of MNMs in living animals. At present, facilitated extraction methods to selectively determine administered MNMs, released metal ion species, or both species, are mostly accessible for environmental and biological media.[62, 68, 157–166]

Given that a biological matrix would interfere in the differentiation of MNMs and released metal ions when using size discrimination strategies, Yu *et al.* proposed the use of Triton-X 114–based CPE to separate AgNPs, polyvinyl pyrrolidone-coated with the hydrodynamic diameter (HD) of 31.4 nm, and $Ag^+$ ions in HepG2 cell lysates.[62] These AgNP-exposed cells, disrupted by sonication and diluted with ultrapure water, were subjected to CPE following the addition of $Na_2S_2O_3$, which assisted the transfer of AgNPs into the Triton-X 114–rich phase through a salt effect and preserved the $Ag^+$ ions in the upper aqueous phase through the formation of hydrophilic complexes. After microwave digestion of each of the two phases, the contents of AgNPs and $Ag^+$ ions were determined through ICP-MS. Yu *et al.* found that the effect of the sonication process on the stability of AgNPs was negligible, and that the transformation of AgNPs into $Ag^+$ ions occurred 24 h post-exposure probably because of the higher ratio of $Ag^+$ ions to AgNPs in the exposed cells (10.3%) than in the pristine AgNP (5.2%) suspension.

In terms of other advanced differentiation methods designed for elucidating MNM dissolution in living animal bodies, we recently developed two chemical differentiation strategies for quantitatively profiling the dissolution and redistribution of AgNPs and QDs in rat liver, spleen, kidney, lung, brain, and blood samples.[68, 71] To facilitate the differentiation procedure, we treated the collected intact rat tissues with Solvable™ solutions, because this excellent solubilizer of wet animal tissues had been demonstrated as the most effective reagent to liberate CNTs from intact biological tissues.[78]

### 3.3.1 PTFE knotted reactor–based differentiation scheme

To study the biodistribution and dissolution behavior of intravenously administered AgNPs [stabilized in 10% FBS/Dulbecco's modified Eagle's medium (DMEM) solution; HD: 68.7 ± 5.2 nm] *in vivo*, we employed homemade knotted reactors (KRs) manufactured from polytetrafluoroethylene (PTFE) tubing to construct a differentiation scheme for quantitative assessment of residual AgNPs and their released $Ag^+$ ions in rat organs and tissues.[68] The on-wall adsorption and retention of metal complexes or precipitates onto filterless KRs was assisted by mixing sample solutions with appropriate complexing or precipitating reagents to ensure that the analyte was readily extractable.[167, 168] The AgNPs, when considered as a form of $Ag^0$ precipitate, should theoretically be retained on the KR's wall, even though they were covered by a thick layer of protein corona. Furthermore, many biomolecules in a biological environment would convert $Ag^+$ ions into KR-extractable species, rather than forming an insoluble AgCl precipitate.[95, 169] Therefore, after optimizing the KR parameters [i.e., the sample acidity and use of a rinsing step to control the stability of absorbed species (both AgNPs and $Ag^+$ ions) on inner wall of KRs], we established critical operating conditions that allowed the retention of released $Ag^+$ ions without contributions from the AgNPs.

Compared with conventional membrane ultrafiltration (MWCO: 3 kDa), our proposed system was tolerant to the Solvable-treated rat tissue and organ samples and provided better accuracy of analytical results. We also applied this differentiation strategy to investigate the biodistribution and dissolution of AgNPs after verifying the equilibrium status of the two Ag species liberated from the solubilized (Solvable-treated) rat tissues and organs. The AgNPs accumulated primarily in the liver and spleen; they then dissolved and released $Ag^+$ ions, which were gradually excreted, resulting in almost all of

the $Ag^+$ ions redistributing to the kidney, lung, and brain during the time interval from one to five days post-administration (Fig. 6). The histopathological evaluation also indicated that inflammatory cell infiltration and focal necrosis were specifically located in the AgNP-rich liver, not in the $Ag^+$-dominated tissues and organs, suggesting that studies of the full chemical fate of AgNPs *in vivo* will be critical for determining their health effects and practical applicability. Our results also indicate that, under well-optimized system conditions, this KR-based differentiation scheme could be a powerful tool for identifying other NMs and their released constituent ions from a variety of biological and environmental media.

### 3.3.2 Chemical vaporization–based differentiation scheme

Although the intrinsic molar ratio of a QD's elements can be used to indicate the integrity of their nanostructures, such measurements are, nevertheless, indirect. To directly quantify the degree of dissolution of CdSeTe/ZnS core/shell QDs (QD705) in living rats, we employed a chemical vapor generation scheme as a novel strategy to selectively vaporize the Te species released from QD705 in Solvable-treated rat samples.[71] The released Te species were chemically converted into volatile hydrogen telluride ($H_2Te$) upon interactions with a strong reducing agent, $NaBH_4$; the native Te species in QD705 could not be vaporized by this applied chemical VG scheme because its oxidation state was already at the lowest level (–2). Furthermore, because the basal concentrations of Te in animal bodies are usually undetected,[170, 171] the Te content is a good tracer for exogenously administered Te-containing QD705. Under the optimized experimental conditions (reductant concentration; HCl concentration in carrier stream; existing biological matrix), the established differentiation system exhibited analytical applicability

and reliability superior to those of the membrane ultrafiltration method (MWCO: 3 kDa). For rats administered intravenously with QD705, we observed (Fig. 7) increased ratios of released Te species to total Te species in blood, liver, and spleen, but a decreased ratio in the kidney, from 2 to 16 weeks post-administration. Accordingly, poly(ethylene glycol)-passivated QD705 progressively dissolves, with a redistribution of its released ionic species occurring in living rat bodies, confirming that studies of the chemical composition and long-term chemical fate of QDs are indispensable when examining their toxicological considerations.

## 4. Perspectives of using ICP-MS techniques for studies of the chemical fate of MNMs

Dissolution of MNMs has been a key process in understanding their cellular toxic responses in biological systems; as such, MNMs, based on their release of ionic species, would have the highest potential to be recognized as hazardous substances. To date, there have been fragmentary accounts of the chemical fate and dissolution behavior of MNMs guiding the consequent toxic responses in living animals. A comprehensive evaluation of MNMs *in vivo* will be necessary to extend our knowledge about their health effects, and to promote their biomedical activities and applications with improved safety and risk assessments. Given the importance of examining MNM dissolution in biological tissues and not just limiting such studies to ICP-MS techniques, there is a great need to develop efficient separation strategies, coupled with adequate sample preparation techniques, to enable characterization of the dissolution of MNMs and determine their chemical fates in living biological systems. Accordingly, the many existing sample preparation and separation techniques for coupling with ICP-MS will need improving, e.g., size calibration and discrimination of dissolved ionic species by using spICP-MS analysis, low recoveries and non-ideal elution behaviors in $AF^4$-ICP-MS systems. Several hurdles for developing new analytical methods/tools must be overcome, including (i) developing appropriate means for liberating residual MNMs and their released metal ion species without changing their original status and (ii) reliably differentiating between pairs of liberated species, having totally different physicochemical properties, coexisting in a biological matrix. Also, to integrate complementary tools, such as transmission electron microscopy, and X-ray spectroscopy can provide supplementary data for revealing MNM

dissolution or transformations in biological tissues with minimal sample destruction. Because increasing numbers of toxicological studies are incorporating dissolution behavior when interpreting the actual biological responses of MNMs, we believe and stress that additional investigations into the chemical fate and dissolution behavior of MNMs will lead to improvements in discerning their nanotoxicity and associated long-term biological effects, and will also benefit the future directions of bio-nanotechnological research.

**Acknowledgment**

We thank Professor Mo-Hsiung Yang for providing helpful advice and the National Science Council of the Republic of China (Taiwan) for financial support (grant 102-2627-M-007-005-MY3).

References


1. E. Hood, *Environ. Health Perspect.*, 2004, **112**, A740–A749.
2. W. G. Kreyling, M. Semmler-Behnke, G. Chaudhry, *Nano Today*, 2010, **5**, 165–168.
3. E. Roduner, *Chem. Soc. Rev.*, 2006, **35**, 583–592.
4. H. Goesmann, C. Feldmann, *Angew. Chem. Int. Ed.*, 2010, **49**, 1362–1395.
5. B. Bhushan, D. Luo, S. R. Schricker, W. Sigmund, S. Zauscher, *Handbook of Nanomaterials Properties*, 2014, Springer
6. D. W. Hobson, *Wiley Interdiscip. Rev. Nanomed. Nanobiotechnol.*, 2009, **1**, 189-202.
7. N. Seltenrich, Environ. Health Perspect., 2013, **121**, A220–A225.
8. H. Liao, Nehl Hafner*Nanomedicine*, 2006, **1**, 201–208.
9. S. Nie, Y. Xing, G. J. Kim, J. W. Simons, *Annu. Rev. Biomed. Eng.*, 2007, **9**, 257–288.
10. N. T. K. Thanh, L. A. W. Green, *Nano Today*, 2010, **5**, 213–230.
11. T. M. Benn, P. Westerhoff, *Environ. Sci. Technol.*, 2008, **42**, 4133–4139.
12. F. Gottschalk, B. Nowack, *J. Environ. Monit.*, 2011, **13**, 1145–1155.
13. K. L. Aillon, Y. Xie, N. El-Gendy, C. J. Berkland, M. L. Forrest, *Adv. Drug Deliv. Rev.*, 2009, **61**, 457–466.
14. H. C. Fischer, W. C. W. Chan, *Curr. Opin. Biotechnol.*, 2007, **18**, 565–571.
15. B. Reidy, A. Haase, A. Luch, K. A. Dawson, I. Lyn, *Materials*, 2013, **6**, 2295–2350.
16. S. Sharifi, S. Behzadi, S. Laurent, M. L. Forrest, P. Stroeve, M. Mahmoudi, *Chem. Soc. Rev.*, 2012, **41**, 2323–2343.
17. K. Luyts, D. Napierska, B. Nemery, P. H. M. Hoet, *Environ. Sci.: Processes Impacts*, 2013, **15**, 23–38.

18. A. Albanese, P. S. Tang, W. C. W. Chan, *Annu. Rev. Biomed. Eng.*, 2012, **14**, 1–16.

19. M. Zhu, G. Nie, H. Meng, T. Xia, A. Nel, Y. Zhao, *Acc. Chem. Res.*, 2013, ***46***, 622–631.

20. J. Liu, Z. Wang, F. D. Liu, A. B. Kane, R. H. Hurt, *ACS Nano*, **2012**, ***6***, 9887–9899.

21. H. S. Choi, W. Liu, P. Misra, E. Tanaka, J. P. Zimmer, B. I. Ipe, M. G. Bawendi, J. V. Frangioni, *Nat. Biotechnol.*, 2007, **25**, 1165–1170.

22. M. Longmire, P. L. Choyke, H. Kobayashi, *Nanomedicine*, 2008, **3**, 703–717.

23. H. S. Choi, W. Liu, F. Liu, K. Nasr, P. Misra, M. G. Bawendi, J. V. Frangioni, *Nat. Nanotechnol.*, 2010, **5**, 42–47.

24. S. K. Misra, A. Dybowska, D. Berhanu, S. N. Luoma, E. Valsami-Jones, *Sci. Total Environ.*, 2012, **438**, 225–232.

25. T. S. Hauck, R. E. Anderson, H. C. Fischer, S. Newbigging, W. C. W. Chan, *Small*, 2010, **6**, 138–144.

26. K. T. Yong, W. C. Law, R. Hu, L. Ye, L. Liu, M. T. Swihart, P. N. Prasad, *Chem. Soc. Rev.*, 2013, **42**, 1236–1250.

27. L. Ye, K. T. Yong, L. Liu, I. Roy, R. Hu, J. Zhu, H. Cai, W. C. Law, J. Liu, K. Wang, J. Liu, Y. Liu, Y. Hu, X. Zhang, M. T. Swihart, P. N. Prasad, *Nat. Nanotechnol.*, 2012, **7**, 453–458.

28. F. Benetti, L. Bregoli, I. Olivato, E. Sabbioni, *Metallomics*, 2014, **6**, 729–747.

29. X. He, Y. Ma, M. Li, P. Zhang, Y. Li, Z. Zhang, *Small*, 2013, **9**, 1482–1491.

30. Y. Tsutsumi, Y. Yoshioka, *Nat. Nanotechnol.*, 2011, **6**, 755.

31. N. Khlebtsov, L. Dykman, *Chem. Soc. Rev.*, 2011, **40**, 1647–1671.

32. P. Krystek, *Microchem. J.*, 2012, **105**, 39–43.

33. E. Pic, L. Bezdetnaya, F. Guillemin, F. Marchal, *Anti-Cancer Agents Med. Chem.*, 2009, **9**, 295–303.
34. S. Vallabhajosula, R. P. Killeen, J. R. Osborne, *Semin. Nucl. Med.*, 2010, **40**, 220-241.
35. X. Sun, W. Cai, X. Chen, *Acc. Chem. Res.*, 2015, **48**, 286–294.
36. S. Goel, F. Chen, E. B. Ehlerding, W. Cai, *Small*, 2014, **10**, 3825–3830.
37. W. T. Phillips, B. A. Goins, A. Bao, *WIREs Nanomed. Nanobiotechnol.*, 2008, **1**, 69–83.
38. A. M. Derfus, W. C. W. Chan, S. N. Bhatia, *Nano Lett.*, 2004, **4**, 11−18.
39. J. A. J. Fitzpatrick, S. K. Andreko, L. A. Ernst, A. S. Waggoner, B. Ballou, M. P. Bruchez, *Nano Lett.*, 2009, **9**, 2736–2741.
40. M. Bottrill, M. Green, *Chem. Commun.*, 2011, **47**, 7039–7050.
41. P. Krystek, A. Ulrich, C. C. Garcia, S. Manohar, R. Ritsema, *J. Anal. At. Spectrom.*, 2011, **26**, 1701–1721.
42. F. von der Kammer, P. L. Ferguson, P. A. Holden, A. Masion, K. R. Rogers, S. J. Klaine, A. A. Koelmans, N. Horne, J. M. Unrine, *Environ. Toxicol. Chem.*, 2012, **31**, 32−49.
43. Y. Li, Y. Gao, Z. Chaia, C. Chen, *Metallomics*, 2014, **6**, 220–232.
44. B. Wang, W. Feng, Y. Zhao, Z. Chai, *Metallomics*, 2013, **5**, 793–803.
45. C. Lin, L. W. Chang, H. Chang, M. Yang, C. Yang, W. Lai, W. Chang, P. Lin, *Nanotechnology*, 2009, **20**, 215101.
46. Y. Han, G. Xie, Z. Sun, Y. Mu, S. Han, Y. Xiao, N. Liu, H. Wang, C. Guo, Z. Shi, Y. Li, P. Huang, *J. Nanopart. Res.*, 2011, **13**, 5373–5380.

47. S. H. Crayton, D. R. Elias, A. A. Zaki, Z. Cheng, A. Tsourkas, *Biomaterials*, 2012, **33**, 1509−1519.

48. B. Gulson, H. Wong, *Environ. Health Perspect.*, 2006, **114**, 1486–1488.

49. F. Larner, M. Rehkämper, *Environ. Sci. Technol.*, 2012, **46**, 4149–4158.

50. F. Larner, Y. Dogra, A. Dybowska, J. Fabrega, B. Stolpe, L. J. Bridgestock, R. Goodhead, D. J. Weiss, J. Moger, J. R. Lead, E. Valsami-Jones, C. R. Tyler, T. S. Galloway, M. Rehkämper, *Environ. Sci. Technol.*, 2012, **46**, 12137–12145.

51. E. Jo, G. Seo,; J. T. Kwon, M. Lee, B. C. Lee, I. Eom, P. Kim, K. Choi, *J. Toxicol. Sci.*, 2013, **38**, 525–530.

52. J. A. Tate, A. A. Petryk, A. J. Giustini, P. J. Hoopes, *Proc. SPIE*, 2011, **7901**, 790117.

53. K. Loeschner, N. Hadrup, M. Hansen, S. A. Pereira, B. Gammelgaard, L. H. Moller, A. Mortensen, H. R. Lam, E. H. Larsen, *Metallomics*, 2014, **6**, 330–337.

54. H. L. Hooper, K. Jurkschat, A. J. Morgan, J. Bailey, A. J. Lawlor, D. J. Spurgeon, C. Svendsen, *Environ. Int.*, 2011, **37**, 1111–1117.

55. T. K. Yeh, J. P. Wu, L. W. Chang, M. H. Tsai, W. H. Chang, H. T. Tsai, C. S. Yang, P. Lin, *Nanotoxicology*, 2011, **5**, 91–97.

56. S. Asghari, S. A. Johari, J. H. Lee, Y. S. Kim, Y. B. Jeon, H. J. Choi, M. C. Moon, I. J. Yu, *J. Nanobiotechnol.*, 2012, **10**, 14.

57. K. Loeschner, N. Hadrup, K. Qvortrup, A. Larsen, X. Gao, U. Vogel, A. Mortensen, H. R. Lam, E. H. Larsen, *Part. Fibre Toxicol.*, 2011, **8**, 18.

58. S. Yu, Y. Yin, J. Liu, *Environ. Sci.: Processes Impacts*, 2013, **15**, 78–92.

59. A. Ulrich, S. Losert, N. Bendixen, A. Al-Kattan, H. Hagendorfer, B. Nowack, C. Adlhart, J. Ebert, M. Lattuada, K. Hungerbuhler, *J. Anal. At. Spectrom.*, 2012, **27**, 1120–1130.

60. A. R. Poda, A. J. Bednar, A. J. Kennedy, A. Harmon, M. Hull, D. M. Mitrano, J. F. Ranville, J. Steevens, *J. Chromatogr. A*, 2011, **1218**, 4219–4225.

61. J. G. Coleman, A. J. Kennedy, A. J. Bednar, J. F. Ranville, J. G. Laird, A. R. Harmon, C. A. Hayes, E. P. Gray, C. P. Higgins, G. Lotufo, J. A. Steevens, *Environ. Toxicol. Chem.*, 2013, **32**, 2069–2077.

62. S. Yu, J. Chao, J. Sun, Y. Yin, J. Liu, G. Jiang, *Environ. Sci. Technol.*, 2013, **47**, 3268−3274.

63. J. Jimenez-Lamana, F. Laborda, E. Bolea, I. Abad-Alvaro, J. R. Castillo, J. Bianga, M. He, K. Bierla, S. Mounicou, L. Ouerdane, S. Gaillet, J. Rouanet, J. Szpunar, *Metallomics*, 2014, **6**, 2242–2249.

64. B. Schmidt, K. Loeschner, N. Hadrup, A. Mortensen, J. J. Sloth, C. B. Koch, E. H. Larsen, *Anal. Chem.*, 2011, **83**, 2461–2468.

65. E. P. Gray, J. G. Coleman, A. J. Bednar, A. J. Kennedy, J. F. Ranville, C. P. Higgins, *Environ. Sci. Technol.*, 2013, **47**, 14315–14323.

66. K. Loeschner, M. S. J. Brabrand, J. J. Sloth, E. H. Larsen, *Anal. Bioanal. Chem.*, 2014, **406**, 3845–3851.

67. E. Bolea, J. Jimenez-Lamana, F. Laborda, I. Abad-Alvaro, C. Blade, L. Arola, J. R. Castillo, *Analyst*, 2014, **139**, 914–922.

68. C. K. Su, H. T. Liu, S. C. Hsia, Y. C. Sun, *Anal. Chem.*, 2014, **86**, 8267–8274.

69. A. Robe, E. Pic, H. Lassalle, L. Bezdetnaya, F. Guillemin, F. Marchal, *BMC Cancer*, 2008, **8**, 111.

70. Z. Arslan, M. Ates, W. McDuffy, M. S. Agachana, I. O. Farah, W. W. Yu, A. Bednar, *J. Hazard. Mater.*, 2011, **192**, 192–199.

71. C. K. Su, T. Y. Cheng, Y. C. Sun, *J. Anal. At. Spectrom.*, 2015, **30**, 426–434.

72. K. Loeschner, J. Navratilova, C. Købler, K. Mølhave, S. Wagner, F. von der Kammer, E. H. Larsen, *Anal. Bioanal. Chem.*, 2013, **405**, 8185–8195.

73. R. J. B. Peters, Z. H. Rivera, G. van Bemmel, H. J. P. Marvin, S. Weigel, H. Bouwmeester, *Anal. Bioanal. Chem.*, 2014, **406**, 3875–3885.

74. A. M. P. Neto, R. A. S. de Souza, A. D. Leon-Nino, J. D. A. da Costa, R. S. Tiburcio, T. A. Nunes,; T. C. S. de Mello, F. T. Kanemoto, F. M. P. Saldanha-Corrêa, M. F. Gianesella, *Renew. Energy*, 2013, **55**, 525–531.

75. J. Pan, C. Zhang, Z. Zhang, G. Li *Anal. Chim. Acta*, 2014, **815**, 1–15.

76. Z. Zhong, F. Chen, A. S. Subramanian, J. Lin, J. Highfield, A. Gedanken, *J. Mater. Chem.*, 2006, **16**, 489–495.

77. D. Radziuk, D. Grigoriev, W. Zhang, D. Su, H. Möhwald, D. Shchukin, *J. Phys. Chem. C*, 2010, **114**, 1835–1843.

78. K. Doudrick,; N. Corson, G. Oberdorster, A. C. Eder, P. Herckes, R. U. Halden, P. Westerhoff, *ACS Nano*, 2013, **7**, 8849–8856.

79. J. A. Nóbrega, M. C. Santos, R. A. de Sousa, S. Cadore, R. M. Barnes, M. Tatro, *Spectroc. Acta Pt. B-Atom. Spectr.*, 2006, **61**, 465–495.

80. C. M. Tseng, A. de Diego, F. M. Martin, D. Amouroux, O. F. X. Donard, *J. Anal. At. Spectrom.*, 1997, **12**, 743–750.

81. G. Tao, S. N. Willie, R. E. Sturgeon, *Analyst*, 1998, **123**, 1215–1218.

82. J. Szpunar, *Trac—Trends Anal. Chem.*, 2011, **19**, 127–137.

83. S. Kascakova, B. Kruijt, H. S. de Bruijn, A. van der Ploeg-van den Heuvel, D. J. Robinson, H. J. C. M. Sterenborg, A. Amelink, *J. Photochem. Photobiol. B-Biol.*, 2008, **91**, 99–107.

84. H. Sawada, K. Korenaga, N. Kawamura, H. Mizu, H. Yamauchi, *Chromatography*, 2011, **32**, 121–126.

85. B. Kowalczyk, I. Lagzi, B. A. Grzybowski, *Curr. Opin. Colloid Interface Sci.*, 2011, **16**, 135–148.

86. J. Liu, S. Yu, Y. Yin, J. Chao, *Trac—Trends Anal. Chem.*, 2013, **33**, 95–106.

87. M. Hadioui, S. Leclerc, K. J. Wilkinson, *Talanta*, 2013, **105**, 15–19.

88. A. Chatterjee, M. Santra, N. Won, S. Kim, J. K. Kim, S. B. Kim, K. H. Ahn, *J. Am. Chem. Soc.*, 2009, **131**, 2040–2041.

89. M. A. Maurer-Jones, M. P. S. Mousavi, L. D. Chen, P. Buhlmann, C. L. Haynes, *Chem. Sci.*, 2013, **4**, 2564–2572.

90. A. Fabricius, L. Duester, B. Meermann, T. A. Ternes, *Anal. Bioanal. Chem.*, 2014, **406**, 467–479.

91. I. Lynch, K. A. Dawson, *Nano Today*, 2008, **3**, 40–47.

92. M. Lundqvist, J. Stigler, G. Elia, I. Lynch, T. Cedervall, K. A. Dawson, *Proc. Natl. Acad. Sci. U. S. A.*, 2008, **105**, 14265–14270.

93. M. Mahmoudi, I. Lynch, M. R. Ejtehadi, M. P. Monopoli, F. B. Bombelli, S. Laurent, *Chem. Rev.*, 2011, **111**, 5610–5637.

94. M. P. Monopoli, C. Åberg, A. Salvati, K. A. Dawson, *Nat. Nanotechnol.*, 2012, **7**, 779–786.

95. C. Levard, M. Hotze, G. V. Lowry, G. E. Brown, Jr, *Environ. Sci. Technol.*, 2012, **46**, 6900–6914.

96. B. A. Chambers, A. R. M. N. Afrooz, S. Bae, N. Aich, L. Katz, N. B. Saleh, M. J. Kirisits, *Environ. Sci. Technol.*, 2014, **48**, 761–769.

97. C. Degueldre, P. Y. Favarger, *Colloids and Surfaces A: Physicochem. Eng. Aspects*, 2003, **217**, 137–142.

98. J. Tuoriniemi, G. Cornelis, M. Hassellöv, *Anal. Chem.*, 2012, **84**, 3965−3972.

99. H. E. Pace, N. J. Rogers, C. Jarolimek, V. A. Coleman, C. P. Higgins, J. F. Ranville, *Anal. Chem.*, 2011, **83**, 9361–9369.

100. F. Laborda, E. Bolea, J. Jimenez-Lamana, *Anal. Chem.*, 2014, **86**, 2270−2278.

101. C. C. Garcia, A, Murtazin, S, Groh, V. Horvatic, K. Niemax, *J. Anal. At. Spectrom.*, 2010, **25**, 645–653.

102. F. Aureli, M. D'Amato, B. de Berardis, A. Raggi, A. C. Turco, F. Cubadda, *J. Anal. At. Spectrom.*, 2012, **27**, 1540–1548.

103. D. M. Mitrano, J. F. Ranville, A. Bednar, K. Kazor, A. S. Hering, C. P. Higgins, *Environ. Sci.: Nano*, 2014, **1**, 248–259.

104. F. Laborda, J. Jimenez-Lamana, E. Bolea, J. R. Castillo, *J. Anal. At. Spectrom.*, 2013, **28**, 1220−1232.

105. A. Hineman, C. Stephan, *J. Anal. At. Spectrom.*, 2014, **29**, 1252−1257.

106. M. Hadioui, C. Peyrot, K. J. Wilkinson, *Anal. Chem.*, 2014, **86**, 4668−4674.

107. S. Lee, X. Bi, R. B. Reed, J. F. Ranville, P. Herckes, P. Westerhoff, *Environ. Sci. Technol.*, 2014, **48**, 10291−10300.

108. J. W. Olesik, P. J. Gray, *J. Anal. At. Spectrom.*, 2012, **27**, 1143−1155.

109. F. Laborda, J. Jimenez-Lamana, E. Bolea, J. R. Castillo, *J. Anal. At. Spectrom.*, 2011, **26**, 1362–1371.

110. O. Borovinskaya, B. Hattendorf, M. Tanner, S. Gschwind, D. Günther, *J. Anal. At. Spectrom.*, 2013, **28**, 226–233.

111. O. Borovinskaya, S. Gschwind, B. Hattendorf, M. Tanner, D. Günther, *Anal. Chem.*, 2014, **86**, 8142−8148.

112. Y. Su, W. Wang, Z. Li, H. Deng, G. Zhou, J. Xu, X. Ren, *J. Anal. At. Spectrom.*, 2015, **30**, 1184–1190.

113. J. P. Novak, C. Nickerson, S. Franzen, D. L. Feldheim, *Anal. Chem.*, 2001, **73**, 5758–5761.

114. V. Sharma, K. Park, M. Srinivasarao, *Proc. Natl. Acad. Sci. U. S. A.*, 2009, **106**, 4981–4985.

115. G. Chen, Y. Wang, L. H. Tan, M. Yang, L. S. Tan, Y. Chen, H. Chen, *J. Am. Chem. Soc.*, 2009, **131**, 4218–4219.

116. D. Steinigeweg, M. Schutz, M. Salehi, S. Schlucker, *Small*, 2011, **7**, 2443–2448.

117. O. Akbulut, C. R. Mace, R. V. Martinez, A. A. Kumar, Z. Nie, M. R. Patton, G. M. Whitesides, *Nano Lett.*, 2012, **12**, 4060−4064.

118. F. Bonaccorso, M. Zerbetto, A. C. Ferrari, V. Amendola, *J. Phys. Chem. C*, 2013, **117**, 13217−13229.

119. Z. Chen, H. Chen, H. Meng, G. Xing, X. Gao, B. Sun, X. Shi, H. Yuan, C. Zhang, R. Liu, F. Zhao, Y. Zhao, X. Fang, *Toxicol. Appl. Pharmacol.*, 2008, **230**, 364–371.

120. C. Levard, B. C. Reinsch, F. M. Michel, C. Oumahi, G. V. Lowry, G. E. Brown, Jr. *Environ. Sci. Technol.*, 2011, **45**, 5260–5266.

121. K. A. Huynh, K. L. Chen, *Environ. Sci. Technol.*, 2011, **45**, 5564–5571.

122. J. M. Pettibone, J. Gigault, V. A. Hackley, *ACS Nano*, 2013, **7**, 2491–2499.

123. M. C. Mancini, B. A. Kairdolf, A. M. Smith, S. Nie, *J. Am. Chem. Soc.*, 2008, **130**, 10836–10837.

124. T. S. Radniecki, D. P. Stankus, A. Neigh, J. A. Nason, L. Semprini, *Chemosphere*, 2011, **85**, 43–49.

125. M. Horie, K. Fujita, H. Kato, S. Endoh, K. Nishio, L. K. Komaba, A. Nakamura, A. Miyauchi, S. Kinugasa, Y. Hagihara, E. Niki, Y. Yoshida, H. Iwahashi, *Metallomics*, 2012, **4**, 350–360.

126. H. C. Fischer, T. S. Hauck, A. Gomez-Aristizabal, W. C. W. Chan, *Adv. Mater.*, 2012, **22**, 2520–2524.

127. A. Galeone, G. Vecchio, M. A. Malvindi, V. Brunetti, R. Cingolani, P. P. Pompa, *Nanoscale*, 2012, **4**, 6401–6407.

128. L. M. Stevenson, H. Dickson, T. Klanjscek, A. A. Keller, E. McCauley, R. M. Nisbet, *PLoS One*, 2013, **8**, e74456.

129. I. Corazzari, A. Gilardino, S. Dalmazzo, B. Fubini, D. Lovisolo, *Toxicol. Vitro*, 2013, **27**, 752–759.

130. C. Levard, S. Mitra, T. Yang, A. D. Jew, A. R. Badireddy, G. V. Lowry, G. E. Brown, Jr *Environ. Sci. Technol.*, 2013, **47**, 5738−5745.

131. S. A. James, B. N. Feltis, M. D. de Jonge, M. Sridhar, J. A. Kimpton, M. Altissimo, S. Mayo, C. Zheng, A. Hastings, D. L. Howard, D. J. Paterson, P. F. A. Wright, G. F. Moorhead, T. W. Turney, J. Fu, *ACS Nano*, 2013, **7**, 10621–10635.

132. T. Tsai, *J. Chromatogr. B*, 2003, **797**, 161–173.

133. S. V. Deshmukh, A. Harsch, *J. Pharmacol. Toxicol. Methods*, 2011, **63**, 35–39.

134. G. A. Sotiriou, S. E. Pratsinis, *Curr. Opin. Chem. Eng.*, 2011, **1**, 3–10.

135. S. Prabhu, E. K. Poulose, *Int. Nano Lett.*, 2012, **2**, 32.

136. S. Eckhardt, P. S. Brunetto, J. Gagnon, M. Priebe, B. Giese, K. M. Fromm, *Chem. Rev.*, 2013, **113**, 4708–4754.

137. L. Rizzello, P. P. Pompa, *Chem. Soc. Rev.*, 2014, **43**, 1501–1518.

138. C. Mizuno, S. Bao, T. Hinoue, T. Nomura, *Anal. Sci.*, 2005, **21**, 281–286.

139. P. A. Holden, F. Klaessig, R. F. Turco, J. H. Priester, C. M. Rico, H. Avila-Arias, M. Mortimer, K. Pacpaco, J. L. Gardea-Torresdey, *Environ. Sci. Technol.*, 2014, **48**, 10541−10551.

140. E. P. Gray, T. A. Bruton, C. P. Higgins, R. U. Halden, P. Westerhoff, J. F. Ranville, *J. Anal. At. Spectrom.*, 2012, **27**, 1532–1539.

141. K. Tiede, A. B. A. Boxall, D. Tiede, S. P. Tear, H. David, J. Lewis, *J. Anal. At. Spectrom.*, 2009, **24**, 964–972.

142. K. Tiede, A. B. A. Boxall, X. Wang, D. Gore, D. Tiede, M. Baxter, H. David, S. P. Teare, J. Lewis, *J. Anal. At. Spectrom.*, 2010, **25**, 1149–1154.

143. T. A. Hanley, R. Saadawi, P. Zhang, J. A. Caruso, J. Landero-Figueroa, *Spectroc. Acta Pt. B-Atom. Spectr.*, 2014, **100**, 173–179.

144. X. X. Zhou, R. Liu, J. F. Liu, *Environ. Sci. Technol.*, 2014, **48**, 14516–14524.

145. A. Helfrich, W. Bruchert, J. Bettmer, *J. Anal. At. Spectrom.*, 2006, **21**, 431–434.

146. J. Soto-Alvaredo, M. Montes-Bayón, J. Bettmer, *Anal. Chem.*, 2013, **85**, 1316-1321.

147. L. Liu, B. He, Q. Liu, Z. Yun, X. Yan, Y. Long, G. Jiang, *Angew. Chem. Int. Ed.*, 2014, **53**, 14476–14479.

148. B. Franze, C. Engelhard, *Anal. Chem.*, 2014, **86**, 5713−5720.

149. K. D. Caldwell, *Anal. Chem.*, 1988, **17**, 959A–971A.

150. J. G. Giddings, *Science*, 1993, **260**, 1456–1465.

151. P. M-M, A. Siripinyanond, *J. Anal. At. Spectrom.*, 2014, **29**, 1739–1752.

152. D. M. Mitrano, A. Barber, A. Bednar, P. Westerhoff,; C. P. Higgins, J. F. Ranville, *J. Anal. At. Spectrom.*, 2012, **27**, 1131–1142.

153. G. Yohannes, M. Jussila, K. Hartonen, M. L. Riekkola, *J. Chromatogr. A*, 2011, **1218**, 4104–4116.

154. S. K. R. Williams, J. R. Runyon, A. A. Ashames, *Anal. Chem.*, 2011, **83**, 634–642.

155. F. Von der Kammer, S. Legros, E. H. Larsen, K. Loeschner, T. Hofmann, *Trac—Trends Anal. Chem.*, 2011, **30**, 425–436.

156. J. Gigault, J. M. Pettibone, C. Schmitt, V. A. Hackley, *Anal. Chim. Acta*, 2014, **809**, 9–24.

157. J. Liu, J. Chao, R. Liu, Z. Tan, Y. Yin, Y. Wu, G. Jiang, *Anal. Chem.*, 2009, **81**, 6496–6502.

158. J. B. Chao, J. F. Liu, S. J. Yu, Y. D. Feng, Z. Q. Tan, R. Liu, Y. Q. Yin, *Anal. Chem.*, 2011, **83**, 6875–6882.

159. L. Li, K. Leopold, M. Schuster, *Chem. Commun.*, 2012, **48**, 9165–9167.

160. L. Li, K. Leopold, *Anal. Chem.*, 2012, **84**, 4340–4349.

161. L. Li, G. Hartmann, M. Döblinger, M. Schuster, *Environ. Sci. Technol.*, 2013, **47**, 7317−7323.

162. C. K. Su, Y. C. Sun, *Nanoscale*, 2013, **5**, 2073–2079.

163. S. Su, B. Chen, M. He, Z. Xiao, B. Hu, *J. Anal. At. Spectrom.*, 2014, **29**, 444–453.

164. G. Hartmann, T. Baumgartner, M. Schuster, *Anal. Chem.*, 2014, **86**, 790−796.

165. C. K. Su, C. W. Huang, C. S. Yang, Y. J. Wang, Y. C. Sun, *Anal. Chem.*, 2010, **82**, 7096–7102.

166. C. K. Su, C. W. Huang, Y. C. Sun, *Toxicol. Lett.*, 2014, **227**, 84–90.

167. S. Cerutti, L. D. Martinez, R. G. Wuilloud, *Appl. Spectrosc. Rev.*, 2005, **40**, 71–101.

168. X. Yan, Y. Jiang, *Trac—Trends Anal. Chem.*, 2001, **20**, 552–562.

169. A. Ostermeyer, C. K. Mumuper, L. Semprini, T. Radniecki, *Environ. Sci. Technol.*, 2013, **47**, 14403–14410.

170. L. M. Klevay, *Pharmac. Ther. A*, 1976, **1**, 223–229.

171. Y. Ogra, R. Kobayashi, K. Ishiwata, K. T. Suzuki, *J. Inorg. Biochem.*, 2008, **102**, 1507–1513.

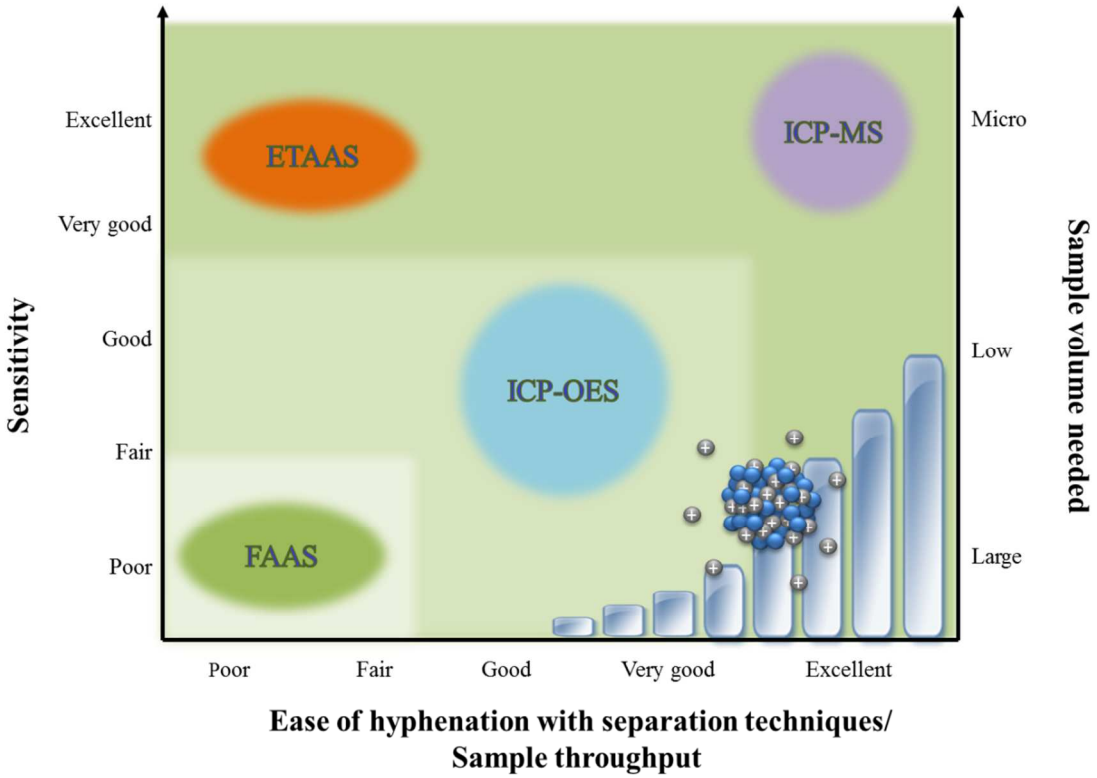


**Fig. 1.** Analytical characteristics of conventional elemental analysis instruments for studying chemical fate and dissolution behaviors of MNMs in biological tissues.

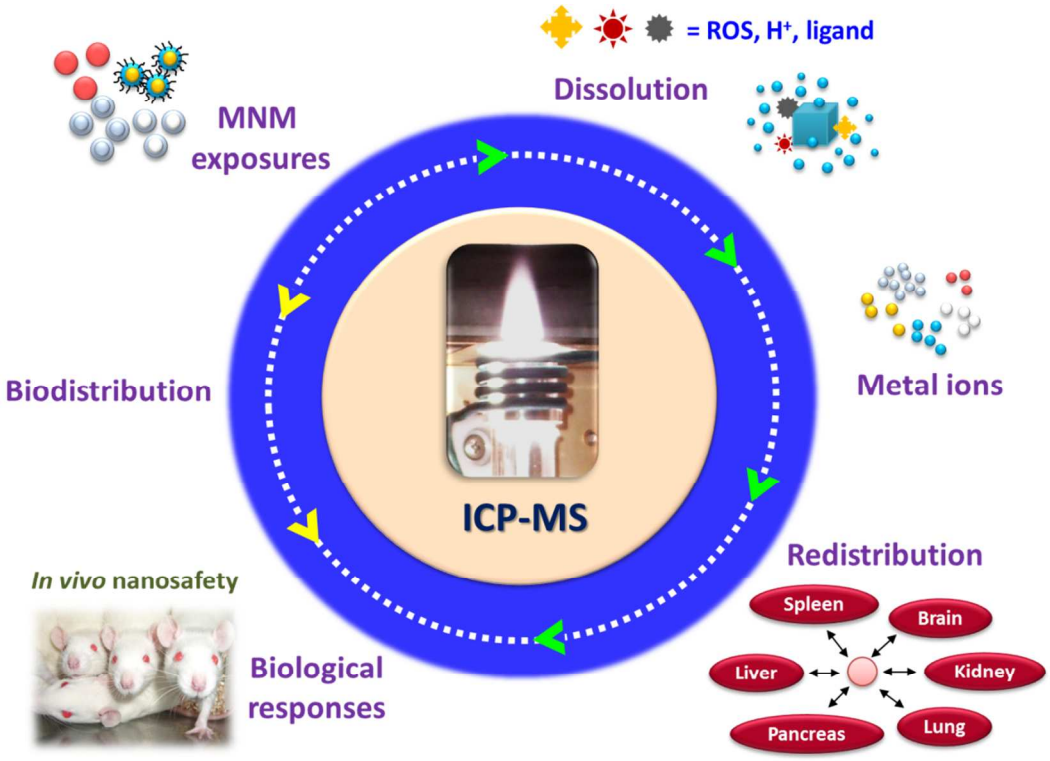


**Fig. 2.** A schematic representation illustrating the interrelations among NMN exposure, dissolution, distribution, and induced biological responses.

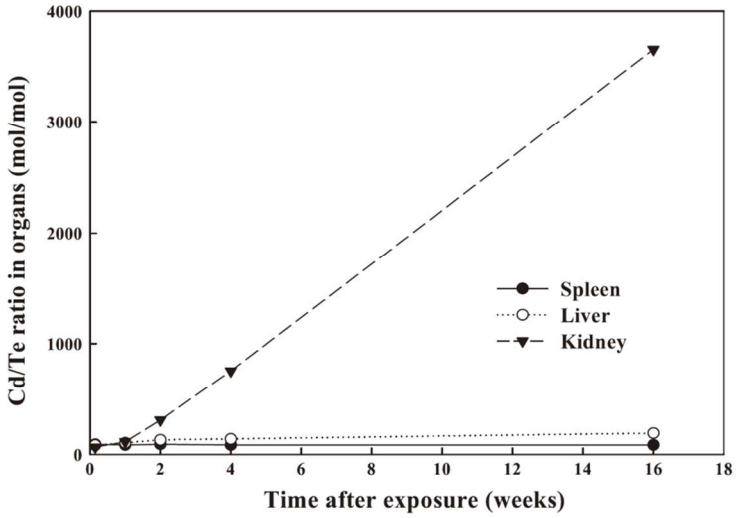


**Fig. 3.** A time course study on changes of Cd/Te molar ratio (Cd/Te ratio) in the spleen, liver and kidneys of ICR mice treated with 40 $\mu$mol of QD705. While no significant change in Cd/Te ratio was observed in the spleen and liver over 16 weeks, the Cd/Te ratio increased sharply in the kidneys, indicating that there was a steady disintegration of the QD705 complex with release of Cd in the kidneys but not in the spleen and liver. Reprinted with permission from ref. 45. Copyright 2009 IOP Publishing Ltd.

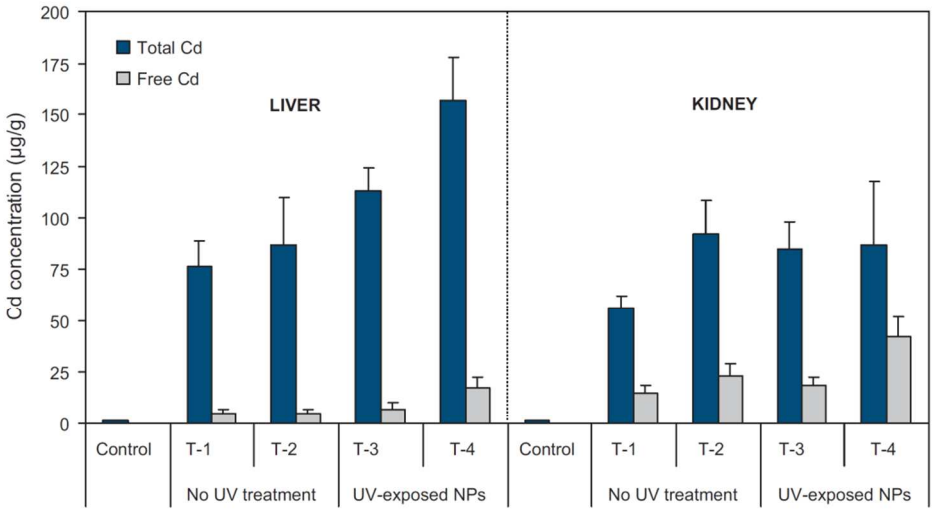


**Fig. 4.** Distribution of NPs and free Cd in the liver and kidney samples from rats exposed to thiol-capped CdSe NPs. The results are average ± standard deviation (dry-weight) from six rats for each treatment (n = 6, control, T-1, T-2, T-3 and T-4). Total Cd levels were higher in the liver than kidney. Free Cd ions accumulated in the kidney. Note that free Cd is present in both liver and kidney even NPs were not exposed UV-light (365 nm). Deliberate exposures of NPs to UV-light elevated the levels of NPs and free Cd in the organs. Reprinted with permission from ref. 70. Copyright 2011 Elsevier.

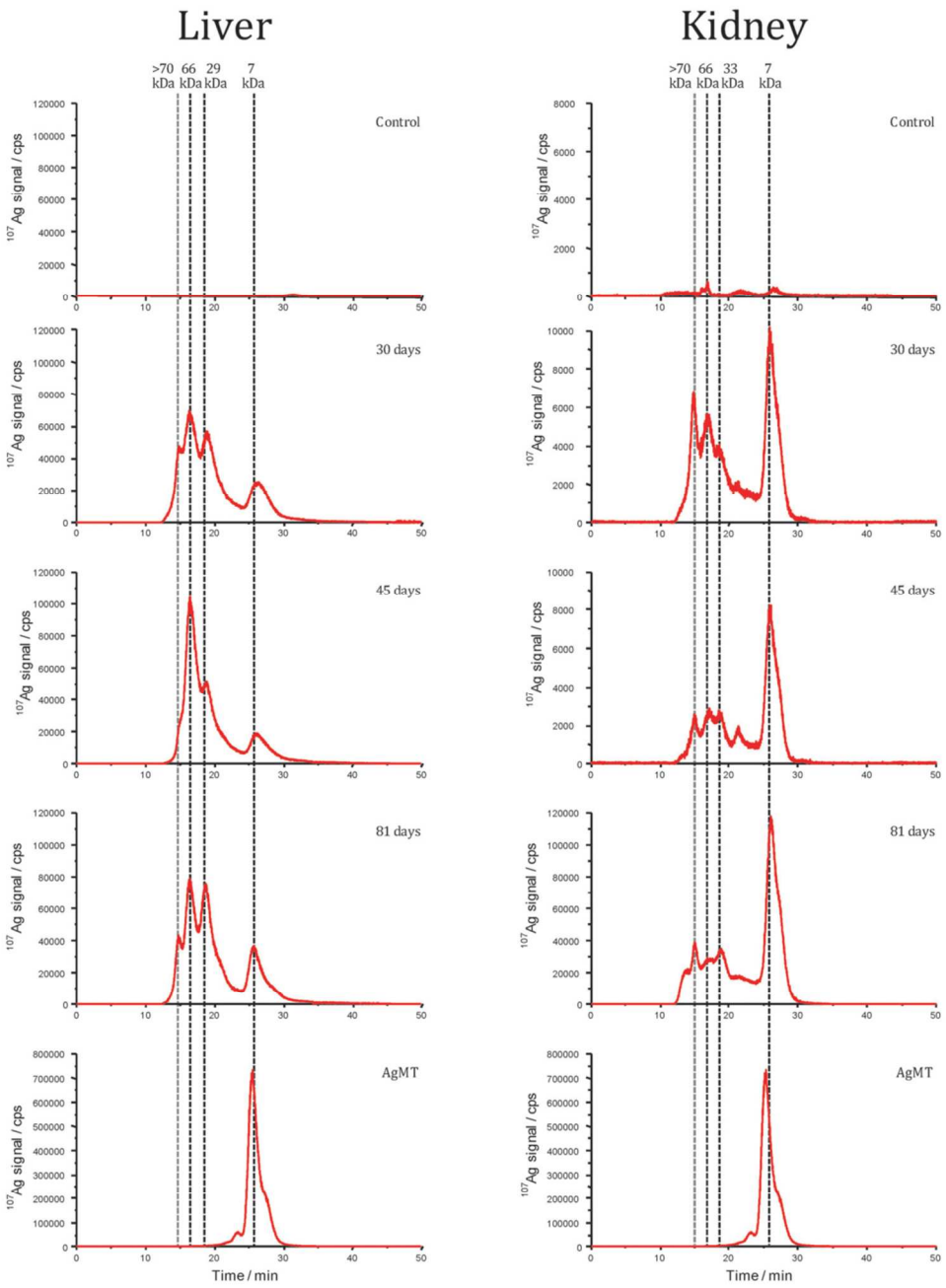


**Fig. 5.** $^{107}$Ag signal obtained for cytosols extracted from the liver and kidney from experiments at 30, 45 and 81 days compared with the MT standard spiked with silver. Reprinted with permission from ref. 63. Published by The Royal Society of Chemistry.

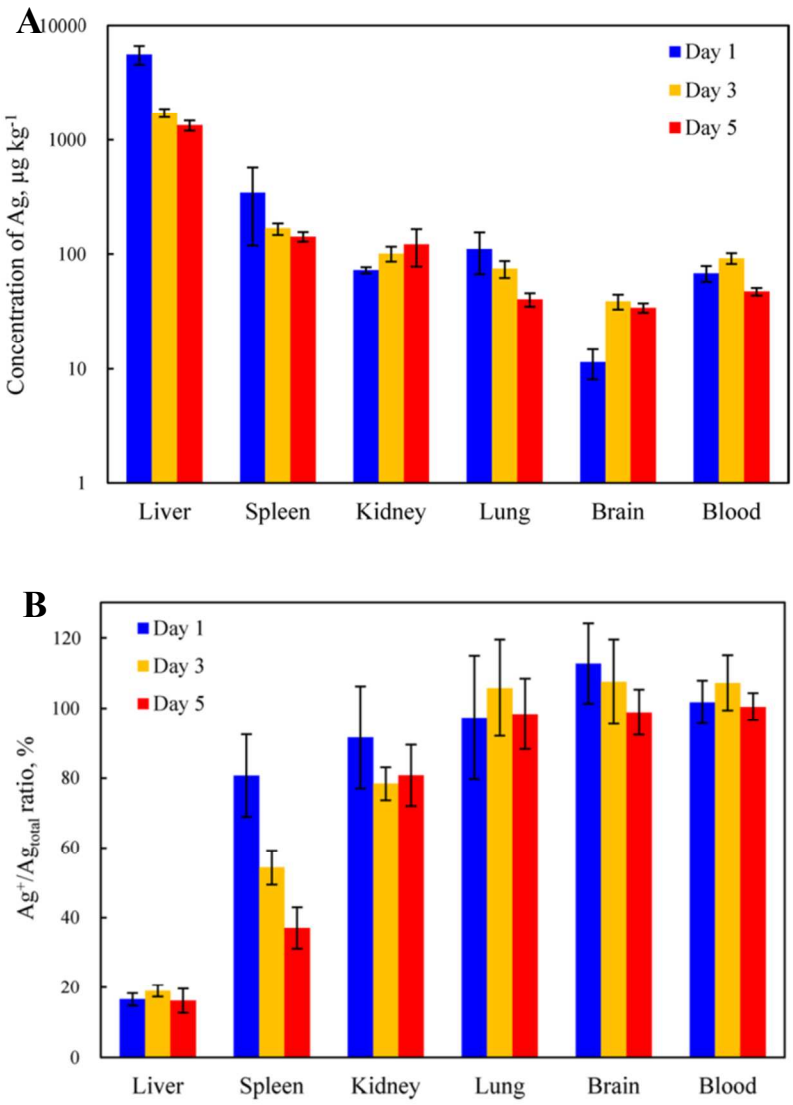


**Fig. 6.** Quantitative biodistribution and dissolution profiles of AgNPs one, three, and five days post-administration in living rats (500 μg $kg^{-1}$ body weight; $n$ = 4). (A) Total Ag concentrations in rat organs/tissues determined using our developed KR-based sample pretreatment scheme with the sample solubilized in Solvable™. (B) Dissolution kinetics of the administered AgNPs *in vivo*, represented with respect to $Ag^{+}/Ag_{total}$ ratios. Reprinted with permission from ref. 68. Copyright 2014 American Chemical Society.

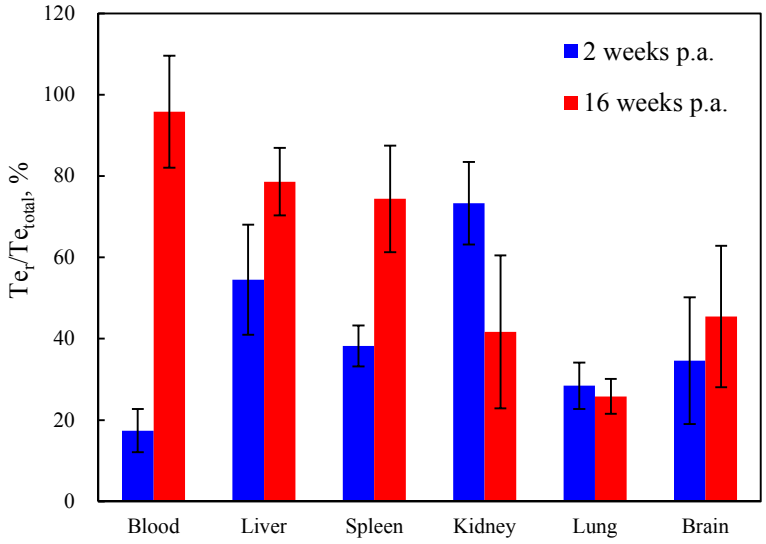


**Fig. 7.** Quantitative dissolution behavior of QD705 2 and 16 weeks post-administration in living rats (200 pmol $kg^{-1}$ body weight; $n$ = 4) represented with respect to $Te_r/Te_{total}$ ratios. Reproduced with permission from ref. 71. Copyright 2015 The Royal Society of Chemistry.

**Table 1**. Available sample pretreatment methods developed to allow the characterization of MNMs or released ions in biological tissues

| Method | MNM | Sample | Treatment procedure | Ref. |
|---|---|---|---|---|
| Sonication | AgNPs | *L. variegatus* | 1 g of frozen tissue was added to 10 mL of deionized water and sonicated for 1 h; then the treated sample was centrifuged to remove biological debris | 60 |
| Sonication | AgNP | *L. variegatus* | deionized water (1 mL) was added to approximately 1 g of *L. variegatus* homogenate and sonicated for 1 h; the treated sample was centrifuged and filtered (0.45 μm) to remove biological debris | 61 |
| Sonication | AgNP | HepG2 cell | The obtained cells were disrupted by sonication and adjusted to a fixed volume by adding ultrapure water | 62 |
| Sonication | AgNP | Rat liver and kidney | A 0.7 g sample was ground in liquid nitrogen; a volume of 2 mL of 200 mM ammonium acetate (pH 7.5) buffer containing 1 mM dithiothreitol and 0.1 mM phenylmethylsulfonylfluoride was added and the solution was sonicated for 1.5 min; the supernatant was collected as the mixture was centrifuged at 4 °C for 20 min at 120000 g | 63 |
| Alkaline | AuNP | Rat liver | Rat liver samples were first homogenized in water | 64 |

| | | | | |
|---|---|---|---|---|
| | | | [10% (w/w)] and stabilized with excess amount of BSA; then the homogenized samples were treated with TMAH [5% (v/v)], sonicated for 1 h, and mechanically rotated overnight at room temperature | |
| Alkaline | AuNP AgNP | Ground beef, *D. magna*, and *L. variegatus* | 0.5 g tissue (beef and *L. variegatus*) or approximately 1.75 mg *D. magna* were treated with 10 mL of TMAH solution and bath sonicated for 1 h; the treated samples were allowed for digestion between 12 and 24 h; digested samples were diluted to produce a final maximum TMAH concentration of 1% before analysis | 65 |
| Alkaline | AuNP | Rat spleen | The rat spleens were physically homogenized and sonicated for 1 h, and TMAH solution was added to a final concentration of 5 % (v/v); BSA solution was added to allow the formation of a BSA monolayer on AuNP surfaces; the final samples were sonicated for 1 h and rotated mechanically at room temperature overnight | 66 |
| Alkaline | AgNP | HepG2 cell | One culture plate was added with 4 mL of TMAH and 1 mL of Triton X-100 (0.25%) and rotated mechanically at room temperature for 4 h | 67 |
| Alkaline | AgNP | Rat feces | A 100 mg ground sample was treated with 2 mL of | 63 |

| | | | | |
|---|---|---|---|---|
| | | | 25% TMAH (w/w) and 400 μL of 0.5% cysteine (w/w); the treated solution was made up to 10 mL with a solution of 0.1% cysteine and 0.05% Triton X-100 (w/w), sonicated for 1 min, and centrifuged at 21 °C at 3000 rpm for 15 min | |
| Alkaline | AgNP | Rat blood, liver, spleen, kidney, lung, and brain | Rat samples (ca. 50 mg) were solubilized in the Solvable solution (1:9 dilution, w/v) and placed in an oven for 2 h (60 °C); an additional 20-fold (v/v) dilution of the treated samples with 10% FBS/DMEM solution was then demanded to stabilize the AgNPs and $Ag^+$ | 68 |
| Alkaline | CdSe/ZnS QD | Rat liver, spleen, kidney, lung, and axillary lymph node | Organ samples were proportionally added with the Solvable solution (0.5 mL for a weight ≤ 50 mg, 1.0 mL for a weight ≤ 200 mg and 1.5 mL for a weight ≤ 300 mg) and incubated at 50°C until the samples become soluble | 69 |
| Alkaline | CdSe QD | Rat liver, kidney | Liver and kidney samples were (ca. 0.25 g) were digested with 4 mL of 25% TMAH (m/v) at 70 °C for 2 h | 70 |
| Alkaline | CdSeTe/ZnS QD | Rat blood, liver, spleen, kidney, lung, and brain | Rat samples (ca. 100 mg) were dissolved by tenfold (w/v) dilution with the Solvable solution and maintained at 60 °C for 2 h.; an additional 20-fold dilution of the homogenized samples using | 71 |

| | | | | |
|---|---|---|---|---|
| | | | PBS solution was necessary to eliminate the biological matrix effect | |
| Enzyme | AuNP | Rat spleen | A volume of 1.88 mL of digestion buffer (10 mM Tris, 0.5 % SDS, and 1 mM calcium acetate) was added to 100 μL of homogenized spleen samples; the treated samples were vortexed for 10 s, and 20 μL of the diluted enzyme solution (100 U/mL) was added; the final samples were sonicated for 1 h and rotated mechanically at room temperature overnight | 66 |
| Enzyme | AgNP | Chicken meat | 0.25 g meat paste spiked with AgNP suspension was vortexed for 1 min at 2500 rpm and added with 5 ml of the Proteinase K solution [3 mg $mL^{-1}$ in 50 mM ammonium bicarbonate buffer (pH 7.4)]; the mixture was incubated at 37 °C in a water bath for approximately 40 min | 72 |
| Enzyme | AgNP | Chicken meat | A 200-mg sample was buffered with 4 mL of the digestion buffer, vortexed for 1 min, and sonicated for 5 min; a 25-μL proteinase K (822 U $mL^{-1}$) was added to the treated samples and incubated at 35 °C for 3 h | 73 |